

# A BE-SOI MEMS for Inertial Measurement in Geophysical Applications

Bruno Andò, Salvatore Baglio, Gaetano L'Episcopo, Vincenzo Marletta, Nicolò Savalli, and Carlo Trigona

**Abstract**—In this paper, an inertial transducer developed in bulk and etch silicon-on-insulator microelectromechanical-system technology is presented. The device is suitable for low-frequency observation and could represent an interesting solution to implement low-cost monitoring systems for applications requiring a large number of monitoring sites and disposable devices. In particular, the sensor design and the technology adopted are presented here along with models describing the device operation. In addition, an experimental sensor prototype is proposed, and experimental results confirming the suitability of the proposed architecture and its consistence with the predicted behavior are discussed.

**Index Terms**—Bulk and etch silicon-on-insulator (BE-SOI), inertial sensor, low cost, microelectromechanical system (MEMS), seismic measurements, volcanic monitoring.

## I. INTRODUCTION

IT IS established that microelectromechanical system (MEMS) devices are now becoming ubiquitous. They have registered an unprecedented growth in the market and can cater for a large spectrum of applications ranging from environmental monitoring and security to automation, mobile communication, and healthcare, and lately, they have penetrated the sector of game consoles. Although MEMS devices have become popular because they can be produced using the traditional technologies used for integrated circuits, many dedicated technologies have been developed to enhance the device performance and to enable the development of new structures to produce large numbers of low-cost devices.

The characteristics of the MEMS make it suitable for wireless sensor networks. In the related work, the utility of MEMS devices for geophysical sensing, replacing traditional geophones, have been investigated [1]–[3].

The dynamics of volcanic systems are governed by complex coupled phenomena. Understanding these phenomena is a prerequisite for the following: 1) a more robust definition of volcanic alert levels, allowing more efficient and effective volcano monitoring; and 2) a better knowledge of the physical and chemical processes of mass transfer, which is essential for volcanic hazard evaluation [4].

Among the available techniques, seismic, ground deformation, and gas monitoring have been more extensively utilized at active volcanic sites [5]–[7].

Devices utilizing inertial systems (seismometers) are utilized to study the seismicity driven by volcanic processes. Other devices, which are also exploiting inertial systems (spring gravimeters), are employed to study the changes of the gravity field associated with the magma/gas dynamics in the shallower part of a volcano's plumbing system [8], [9].

Volcanic tremor and long period seismicity are typical seismic signatures accompanying eruptive processes [5]. Volcanic tremor is the persistent ground vibration often observed at many volcanoes.

Coupled seismic/gravity studies are limited by issues related to the available instrumentation. In particular, the high cost of spring gravimeters prevents the development of extended arrays of continuously running devices since only a few single institutions can afford the related costs. Furthermore, the harsh conditions often encountered on the summit zone of active volcanoes (limited accessibility, presence of corrosive gases, high daily and seasonal temperature changes, lack of mains electricity, etc.) often pose severe constraints on the use of relatively heavy, sensitive, and delicate instruments, requiring a large amount of power to function [10].

The above shortcomings could be overcome by a “smart dust” approach adopting inertial sensors that are cheaper and lighter and that have lower resource consumption than the existing ones at the expense of poor performance, particularly in terms of sensitivity. The possibility of realizing a network of such low-cost devices within the area to be monitored will produce a large amount of information with a high spatial resolution, which could be useful in implementing an early warning system. The information collected by the network could be used to build qualitative knowledge of the seismic activity in the monitored area, which can successively be refined by having conventional monitoring stations accomplishing fine measurements in specific sites of interest (highlighted by the early warning system).

In this paper, an inertial transducer developed at the Dipartimento di Ingegneria Elettrica, Elettronica e dei Sistemi laboratories by a bulk and etch silicon-on-insulator (BE-SOI) MEMS technology is presented [12]–[15]. The device represents an interesting solution for the implementation of low-cost systems for the monitoring of the seismic activity in volcanic areas. As compared with traditional solutions, the sensing architecture proposed is suited for the implementation of cheap and efficient devices at the expense of sensitivity. This approach allows for the realization of low-cost distributed networks of monitoring

Manuscript received June 19, 2010; revised December 31, 2010; accepted January 3, 2011. The Associate Editor coordinating the review process for this paper was Thomas Lipe.

The authors are with the Dipartimento di Ingegneria Elettrica, Elettronica e dei Sistemi, University of Catania, 95125 Catania, Italy (e-mail: bruno.ando@diees.unict.it).

Digital Object Identifier 10.1109/TIM.2011.2108077

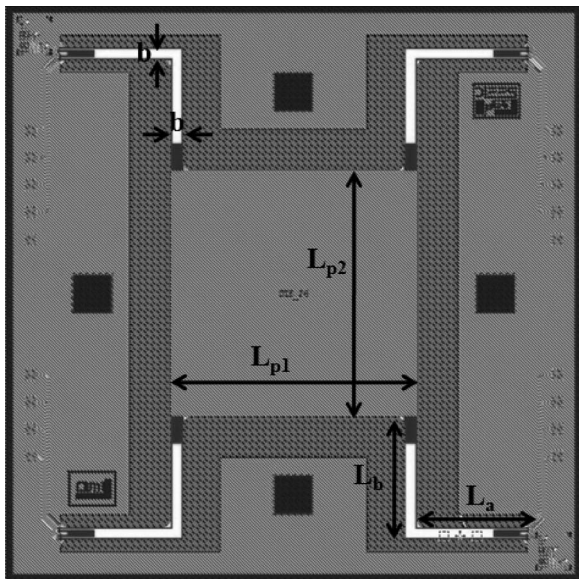


Fig. 1. Layout of the MEMS device. The device has a crab-leg structure with dimensions  $L_a = 618 \mu\text{m}$ ,  $L_b = 2200 \mu\text{m}$ , and  $L_{p1} = L_{p2} = 3000 \mu\text{m}$ .

nodes that implement an early warning system on a large area with a spatial resolution that is unattainable by standard monitoring systems.

## II. BE-SOI MEMS INERTIAL SENSOR

### A. Architecture and FEM Simulations

The investigated device, shown in Fig. 1, has been designed to enhance its sensitivity. Essentially, the device is a suspended square-shaped mass supported by four crab-leg beams. To cope with the above requirements, a proof mass with a size of  $3000 \mu\text{m}$  by  $3000 \mu\text{m}$  has been designed, while the crab-leg beams have the following dimensions:  $b = 183 \mu\text{m}$ ,  $L_a = 618 \mu\text{m}$ , and  $L_b = 2200 \mu\text{m}$  for the thigh and the shin segments, respectively. A large mass and the crab-leg beams have been adopted to enhance the device sensitivity.

The device was designed in the MEMS Pro environment, and the resulting layout is shown in Fig. 1. Four polysilicon (poly-Si) strain gauges  $SG_i$  ( $i = 1, \dots, 4$ ) have been integrated into the beams to measure the structural deformation due to external forces, thus implementing a resistive-readout strategy.

Finite-element method (FEM) simulations have been performed by the CoventorWare suite to investigate the device behavior. By modeling the device response to an imposed stimulus, a resonance frequency,  $\omega_n^{\text{FEM}}$  close to 190 Hz, and a spring stiffness  $k^{\text{FEM}} = 14.39 \text{ N/m}$  have been estimated. If required, this value can be modified during the design phase by modifying the central mass dimensions or the spring properties.

Since the target of this explorative phase is the investigation of the applicability of this MEMS architecture in the aforementioned context, constraints on the frequency response are not strictly addressed. Moreover, it must be considered that this device must be operated in the resonant mode. From an operative point of view, this will require the need to force the device into its resonant regime and to extract the information on the detected quantities by demodulating the output signal and taking the frequency response of the device into account. The

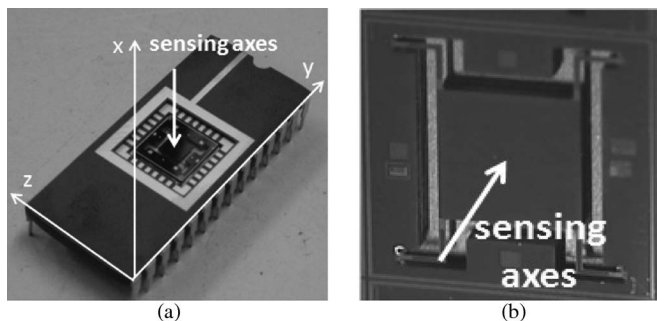


Fig. 2. Real view of the device. (a) The packaged device and (b) a SEM image of the suspended mass.

information about an external stimulus (velocity) is contained in the harmonics around the resonant frequency.

An interesting behavior is observed when the device operates in a real situation and is driven in its resonant mode by natural vibrating sources coming from the monitored environment. In particular, this operating mode could be exploited in monitoring sites offering continuously vibrating sources, which could be the case of some seismic areas. This scenario will be further explored in Section IV.

### B. Real Device

A photograph of the packaged device and a scanning electron microscope (SEM) image of the die with the suspended mass are shown in Fig. 2, where the arrow shows the direction of the sensing axes.

The investigated micromachined device has been realized by using a BE-SOI process, which is available at the Centro Nacional de Microelectronica, Barcelona, Spain.

The steps of the technology can be summarized as follows:

- thermal growth of oxide (Diff) on both sides, thickness of  $0.1 \mu\text{m}$ , at  $T = 1100 \text{ }^\circ\text{C}$ ;
- deposition of polysilicon (Poly) on both sides, thickness of  $0.48 \mu\text{m}$ , and reactive-ion etching (RIE) to remove polysilicon on the front side;
- deposition of the oxide between polysilicon and metal (Cont), thickness of  $0.73 \mu\text{m}$ , and RIE of oxides;
- deposition of Al/Cu alloy (Metal) on the front side, thickness of  $0.7 \mu\text{m}$ , and RIE to remove metal on the front side;
- a  $0.5\text{-}\mu\text{m}$ -thick layer of  $\text{SiO}_2$  (Pad) is deposited on the front side by using a plasma-enhanced chemical vapor deposition technique. Poly-Si and  $\text{SiO}_2$  on the backside are removed, and a  $1\text{-}\mu\text{m}$  layer of metal (Al/Cu) on the backside is deposited. The photolithography of  $\text{SiO}_2$  on the front side is performed, and the  $15\text{-}\mu\text{m}$ -thick layer of silicon is removed through a deep RIE;
- RIE of metal, the thickness to be removed is  $1 \mu\text{m}$ , and an etching procedure of the Silicon on the backside, the thickness to be removed is  $450 \mu\text{m}$ ;
- removing metal from the backside and RIE of buried  $\text{SiO}_2$  from the backside, the thickness to be removed is  $2 \mu\text{m}$ .

The need to have a large mass to enhance the device sensitivity required the choice of this technology, with its seven delicate processing steps, over other processes.

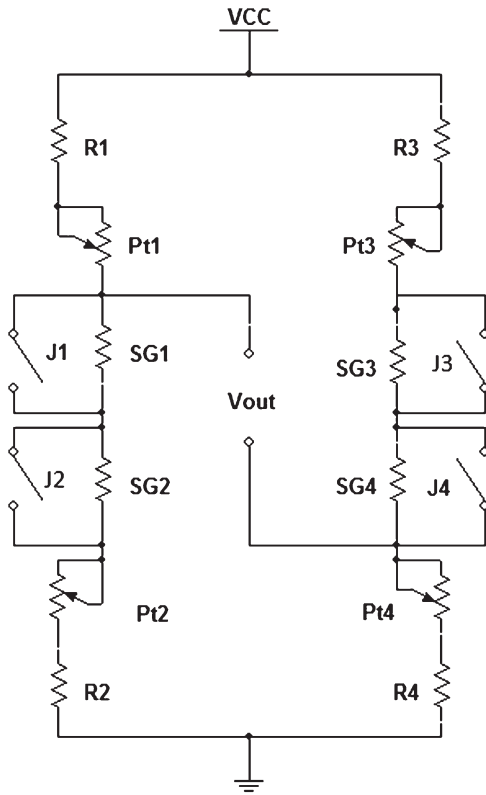


Fig. 3. Wheatstone bridge used to convert the resistance variation in a proportional output voltage signal. The device values are as follows:  $R1 = R4 = 2.2 \text{ k}\Omega$ ;  $R2 = 680 \text{ }\Omega$ ;  $R3 = 1 \text{ k}\Omega$ ;  $SGi = 1.2 \text{ k}\Omega$  ( $i = 1, \dots, 4$ ); and  $V_{cc} = 8 \text{ V}$ .  $Pt_i$  ( $i = 1, \dots, 4$ ) values have been used to balance electronics; switches  $J_i$  ( $i = 1, \dots, 4$ ) have been used to choose the bridge configuration during the development phase. A current value of  $I_{cc} \approx 1.7 \text{ mA}$  has been experimentally estimated.

The proof mass is made of silicon, buried oxide, crystal silicon, and oxides (Diff, Cont, and Pad). Accounting for the geometry and the processing technology, the mass is estimated to be  $10.1 \text{ mg}$ . The crab-leg springs are composed of  $15 \text{ }\mu\text{m}$  of crystal silicon, Diff, Cont and Pad, while  $450 \text{ }\mu\text{m}$  of silicon and the  $2\text{-}\mu\text{m}$  oxide have been removed.

As previously stated, the device uses a resistive-readout strategy. The imposed stimulus  $\dot{x}_i$  results in displacement  $x_o$  of the MEMS structure with respect to the ground and varying resistance  $\Delta R$  of the integrated strain gauges. The experimentally estimated resistance of the strain gauges is around  $1.2 \text{ k}\Omega$ . A direct-current-voltage-driven Wheatstone bridge in the configuration shown in Fig. 3 is used to convert the change in resistance to a proportional voltage signal  $V_{out}$ . The chosen bridge configuration allows for the optimization of the system sensitivity.

Switches  $J_i$  ( $i = 1, \dots, 4$ ) in Fig. 3 have been used to optimize the bridge configuration and for the sake of convenience during the development phase. The bridge has been driven by an  $8 \text{ V}$  supply that supplies to a current of about  $I_{cc} = 1.7 \text{ mA}$  once the values of the devices reported in Fig. 3 are taken into account.

### C. Modeling of the Device

A complete model of the device is described in [15]. This paper will focus on the device behavior when forced by a

velocity term. During the experimental test (see Section IV), the device response will be compared to a reference seismometer installed in the same station.

By considering the readout strategy described in Section II-B, the following assumptions can be made.

- 1) A linear relationship between  $\Delta R$  and  $V_{out}$  can be assumed due to the small expected values of  $\Delta R$ .
- 2) Due to the very small stimulus applied to the device, a linear relationship between the mass displacement  $x_o$  and term  $\Delta R$  can be supposed.

The above assumptions have been supported by experimental results presented in Section III.

On the basis of these considerations and assuming that the mechanical behavior of the device can be described by a second-order model (in terms of  $x_o$  and  $\dot{x}_i$ ), the expected frequency responses in terms of the system output signal  $V_{out}$  is given by the following expression:

$$\frac{V_{out}}{\dot{x}_i} = \frac{sG_x}{\omega_n^2 + \frac{2\xi s}{\omega_n} + 1} \quad (1)$$

where  $V_{out}$  is the output signal of the conditioning electronics processing the information coming from the strain gauge in the bridge arms,  $\dot{x}_i$  is the imposed velocity stimulus,  $G_x$  is the system gain (including the electronics gains and the proportionality factor between  $x_o$  and  $\Delta R$ ),  $\xi$  is the system damping, and  $\omega_n/2\pi$  is the system natural frequency.

### D. Spring Modeling

The device has been modeled by using Castigliano's theorem and considering the strain energy contribution given by the displacement of the structure along the  $x$  axis (see Fig. 2) [16]. The model of the elastic constant has been obtained by using the heterogeneous beam theory that is in accordance with the different stacked materials offered by the technology. For this reason, the device has been studied in a homogeneous domain [16], taking an equivalent shape of the spring into account, having a Young modulus  $E_n$  and moment of inertia  $I_n$ , i.e.,

$$k_m^{est} = \frac{\alpha E_{max} I_n}{l^3} = \frac{\alpha E_{max} b \sum \left[ \frac{E_i t_i^3}{E_n 12} + t_i \frac{E_i}{E_n} (h_i - h_n)^2 \right]}{l^3} \quad (2)$$

where  $\alpha$  is a constant value correlated to the springs;  $E_{max}$  is the maximum Young modulus of the stack materials;  $l$  is the equivalent length of the spring given by a contribution of  $L_a$  and  $L_b$ , as shown in Fig. 1;  $b$  is the width of the beam ( $183 \text{ }\mu\text{m}$ );  $h_n$  is the neutral axis position assumed in the homogeneous domain; and  $E_i$ ,  $t_i$ , and  $h_i$  represent the Young modulus, the thickness, and the neutral axis position for the  $i$ th element, respectively ( $i = 1, \dots, 4$ ). The spring constant  $k_m^{est}$  estimated through the heterogeneous beam theory corresponds to about  $17.01 \text{ N/m}$ . Assuming an equivalent mass  $m = 10.1 \text{ mg}$  leads to a natural frequency of  $\omega_n^{est} = \sqrt{k_m^{est}/m} = 200 \text{ Hz}$ . This frequency assures a good compromise between the need for a large mass that leads to an enhanced sensitivity and a resonant frequency far enough from the frequency range of the expected stimuli.

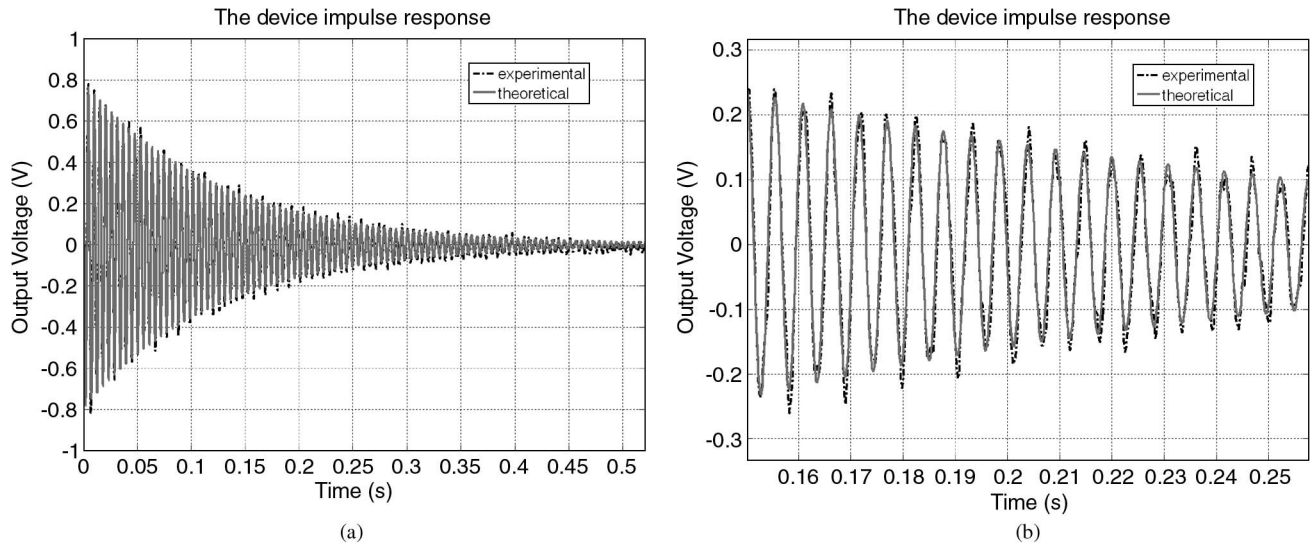


Fig. 4. (a) Experimental impulse response of the device and fitting obtained through model (4). A natural frequency of 186 Hz has been estimated. (b) A zoom of the device impulse response.

The resonant frequency of the device is given by

$$\omega_r = \omega_n \sqrt{1 - 2\xi^2} \quad (3)$$

### III. EXPERIMENTAL OBSERVATIONS OF THE DEVICE BEHAVIOR

The experimental setup for the device characterization consists of a piezoactuated shaker, a structure housing the MEMS device, and a reference laser system OADM 12U6430/S35A adopted to obtain an independent reading of the stimulation imposed on the structure.

Fig. 4(a) shows the impulse response of the device experimentally observed. The observed natural frequency is  $\omega_n^{\text{obs}} = 186$  Hz, which is coherent with values obtained by simulations. The predicted trend for the impulse response is given by

$$V_{\text{out}}^{\text{imp,pred}} = A \cdot \frac{e^{-\xi \cdot \omega_n \cdot t}}{\sqrt{1 - \xi^2}} \sin(\omega_n \cdot t) \quad (4)$$

where  $A$  is the signal amplitude.

By fitting (4) to the observed response in Fig. 4(a) by the Nelder–Mead optimization algorithm [17], the following parameters have been estimated:  $\xi = 0.0069$  and  $A = 0.7975$  V. The following functional  $J$ , computing the root mean square of residuals between the observed response  $V_{\text{out}}^{\text{imp,obs}}$  and the predicted one  $V_{\text{out}}^{\text{imp,pred}}$ , was used by the minimization algorithm:

$$J = \sqrt{\frac{\sum_i^N \left( V_{\text{out}}^{\text{imp,obs}} - V_{\text{out}}^{\text{imp,pred}} \right)^2}{N}} \quad (5)$$

Fig. 4 shows the fitting between the predicted and experimental impulse responses. In order to produce an estimation of the spring stiffness, the following expression has been used:

$$k_m^{\text{obs}} = m \left( \omega_n^{\text{obs}} \right)^2 \quad (6)$$

which leads to  $k_m^{\text{obs}} = 11.25$  N/m.

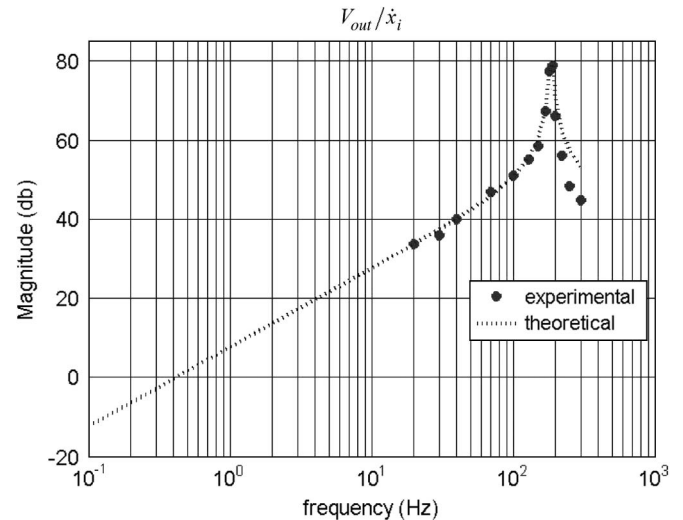


Fig. 5. Frequency response of the MEMS device and comparison between the observed data and the response predicted by model (1).

The oscillation at half the natural frequency superimposed on the main signal is probably due to structural asymmetries arising from the residual stress of the structure produced by the postprocessing technology.

Fig. 5 shows the comparison between the experimentally obtained normalized frequency response  $V_{\text{out}}/\dot{x}_i$  and the expected behavior predicted by model (1). The latter has been fitted by the Nelder–Mead optimization algorithm, which leads to the estimation of parameter  $G_{\dot{x}} = 0.3802$ . Details on the device characterization procedure are given in [15].

The good match between the observed behavior and the expected one makes it possible to confirm the suitability of assumptions in Section II-C, related to the linear behavior of the readout system. Moreover, in future works aimed to characterize the device behavior when operated as a proportional sensor, the linearity features will be further investigated.

The device sensitivity in the working frequency range is obtained from the frequency response in Fig. 5, which is also

TABLE I  
SENSITIVITY VALUES AROUND THE RESONANT FREQUENCY.  $\Delta f$  STATES FOR THE STIMULUS FREQUENCY. HENCE, IT REPRESENTS THE INTERVAL BETWEEN THE RESONANT FREQUENCY AND THE FREQUENCIES AT WHICH THE SENSITIVITY HAS BEEN ESTIMATED

$\Delta f$ (Hz)	Sensitivity (V/m/s)	Resolution (m/s)
0	$1.0 \times 10^4$	$1.0 \times 10^{-6}$
5	$7.5 \times 10^3$	$1.33 \times 10^{-6}$
10	$4.73 \times 10^3$	$2.11 \times 10^{-6}$
20	$2.12 \times 10^3$	$4.74 \times 10^{-6}$

required to estimate the actual stimulus (velocity) in the real scenario, as described in Section IV. It must be borne in mind that the device must be operated in the resonant mode, and as mentioned above, an external stimulus (velocity) will produce harmonics around the resonant frequency. The device sensitivity for some typical frequencies around the resonant mode are reported in Table I.

Table I also gives the device resolution, which has been estimated as the ratio between the observed noise power of the device response  $V_{out}$  in case of a null stimulus and the device sensitivity at some typical frequency.

This analysis leads to a noise-floor estimation of  $1.0 \times 10^{-3} \text{ V}/\sqrt{\text{Hz}}$  at 186 Hz.

Taking into account the resonant behavior of the device, it can be affirmed that the bandwidth of the MEMS device is limited by its natural frequency.

#### IV. TEST IN A REAL SCENARIO

In collaboration with the researchers of the Istituto Nazionale di Geofisica e Vulcanologia (INGV), Sezione di Catania, the device was tested in the field to observe the device behavior in a real scenario. In particular, in June 2009, the device was installed on the summit zone of Stromboli, where a seismic network, managed by the INGV, has been continuously operating. The seismic network is composed of 13 digital stations that are equipped with Guralp CMG 40T broadband sensors (0.02–60 s) [18].

The latter is an ultralightweight seismometer consisting of three sensors in a sealed case, which can measure the north/south, east/west, and vertical components of the ground motion simultaneously, with sensitivity of  $2 \times 400 \text{ V/m} \cdot \text{s}^{-1}$  nominal (differential). Its dimensions are 154 mm in diameter and 207 mm in height [18].

On the basis of the aforementioned features, the Guralp seismometer has been adopted as the reference instrument for the experiment involving the MEMS device.

As already discussed in Section I, the device developed must operate like an event detector, and the aim of the experiment is to assess its features in this working mode. It must be considered that this low-cost device would be suitable for the implementation of sensor networks implementing an early warning system. In this view, the MEMS device is required to provide qualitative information on the ongoing seismic phenomenon rather than a quantitative estimation of its intensity. The latter

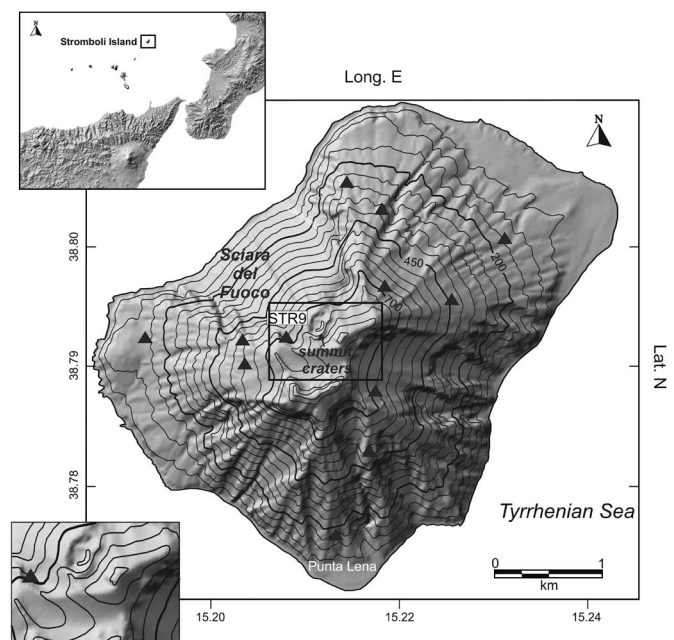


Fig. 6. Topographic map of the island of Stromboli with its seismic network managed by the INGV.

must be accomplished by more accurate and expensive instruments such as the Guralp sensor.

The signal from the seismometers in Stromboli's network is sampled at 50 Hz by 24-bit type recorders (developed by the INGV). Data are transmitted by radio link to local recording centers and then to the INGV monitoring headquarters in Catania, Naples, and Rome.

The MEMS device was deployed within a few meters from the STR9 station (800 m above sea level; about 300 m from the summit craters), as shown in Fig. 6.

The typical volcanic activity of Stromboli consists of intermittent explosions from the summit craters every 10–20 min [19]. Low-frequency seismic signals are associated with the explosions, due to the transient volumetric changes of the plumbing system [20]. Pressure fluctuations, due to the mass transport in the conduits, also induce continuous volcanic tremor [21].

Seismic signals over a wide frequency range are thus recorded by stations on the summit and the flanks of the volcano. The availability of these signals and of a network of calibrated seismic sensors made it possible to test the capabilities of the MEMS device through the comparison between the seismic waveforms recorded by the STR9 station and the MEMS device.

Fig. 7 shows the monitoring site with the experimental setup consisting of the MEMS device, the conditioning circuit, and a Universal Serial Bus data-acquisition (DAQ) device for the personal-computer (PC)-based DAQ system. A LabVIEW tool has been implemented to manage the measurement session. Furthermore, an atomic-clock synchronization tool was used to synchronize the two DAQ systems.

The goal of the experiment was the investigation of the suitability of the device for the development of the distributed sensor network capable of monitoring the volcano seismic

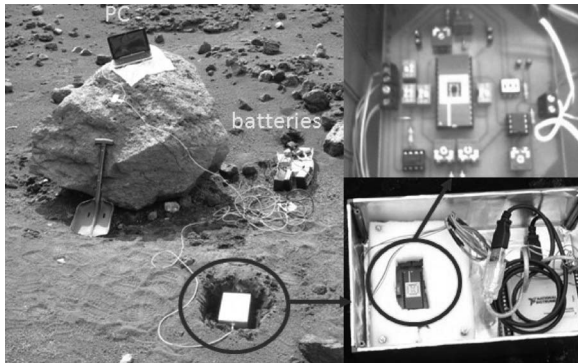


Fig. 7. Case containing the MEMS device and the PC-based DAQ system.

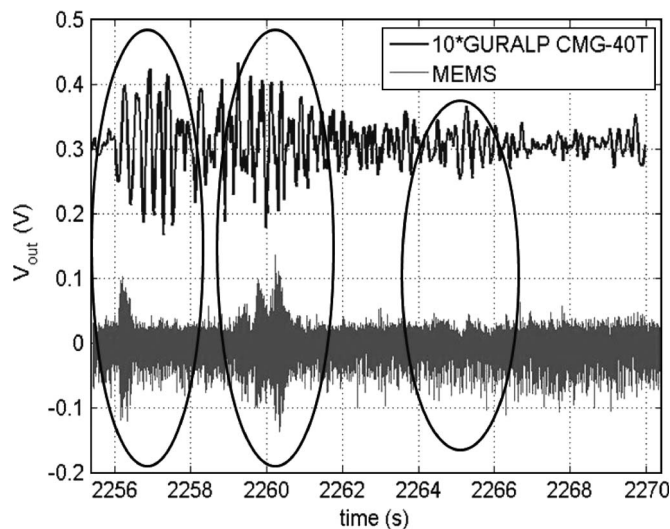


Fig. 8. Example of comparison between the output of the MEMS and Guralp CMG-40T devices (an offset has been added to the Guralp signal for the sake of representation). Both the devices have revealed the events.

activity and providing alerts on the ongoing phenomenon. In the following, experimental results will be discussed, and the comparison between data gathered from the MEMS device and the reference seismometer will be considered.

An example of the recorded data is shown in Fig. 8; both the signals coming from the Guralp (top signal) and MEMS devices (bottom signal) are shown. The signal coming from the Guralp device has been amplified by ten times for the sake of comparison. By observing the two signals, the following conclusions emerge: 1) Both the devices reveal three main events (indicated in Fig. 8) over the basic tremor of the volcano. 2) The MEMS device oscillates at its own natural frequency due to the volcanic tremors, and the three events appear as an amplitude modulation of the main oscillation.

It must be stressed that vibrating sources coming from the monitored environment drive the device in its resonant mode.

The comparison between the output signal of the Guralp device and the demodulated output signal of the MEMS device, shown in Fig. 9, highlights the above statements.

To gain more specific information about the recorded events, the two signals have been analyzed by the wavelet analysis using a dedicated MATLAB toolbox. After the resampling of the two signals, they were decomposed into five levels. Results,

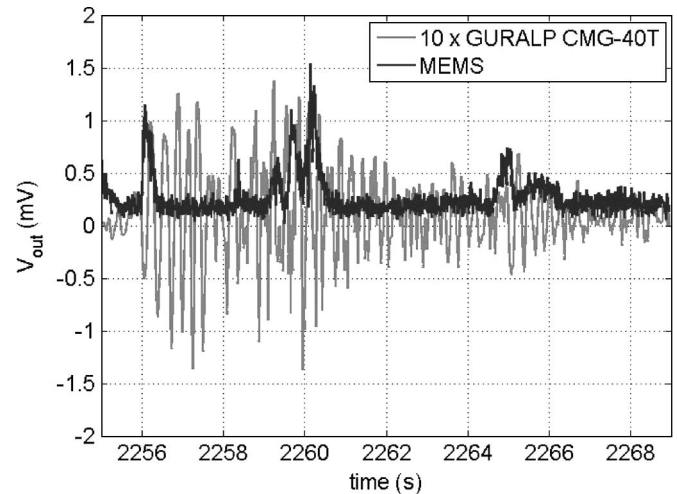


Fig. 9. Comparison between the output signal of the Guralp CMG-40T device and the demodulated output signal of the MEMS device.

shown in Fig. 10, give an evidence of the correlation between the data recorded by the two instruments. Two main events detected by the MEMS device produce a modulation of the resonant behavior, whereas the third event is located in the low-frequency domain.

All three events are also found in the reference device. The different frequency content of the last event suggests that it was triggered by a different volcanic process.

It must be observed that the 50 Hz sampling frequency of the signal coming from the reference station [see Fig. 10(a)] excludes the analysis in the frequency band exceeding 25 Hz.

## V. CONCLUSION

In this paper, an inertial transducer developed in the BE-SOI MEMS technology has been presented. The small device (the proof mass dimensions are 3 mm by 3 mm, and the signal processing electronics can be easily shrunk) could represent an interesting solution to implement a low-cost (compared with high accurate seismometers available on the market) monitoring system for early warning purposes requiring a large number of monitoring sites and disposable devices. At the present state, the sensing methodology, the sensor design, and some aspects of signal conditioning and processing have been taken into account, while several practical aspects, as well as dimensions, geometries, and electronics, must be further investigated before considering this device mature and reliable enough for the market.

The sensor design and the technology adopted have been presented here along with models describing the device operation. Moreover, an experimental sensor prototype has been proposed, and experimental results confirming the suitability of the proposed architecture and its consistence with the predicted behavior have been discussed. As expected, features of the MEMS sensor (e.g., compare specifications in Table I with those declared for the Guralp CMG-40T seismometer), including costs, allow for the implementation of a low-cost distributed network using the MEMS devices such as event detectors providing qualitative information on the observed

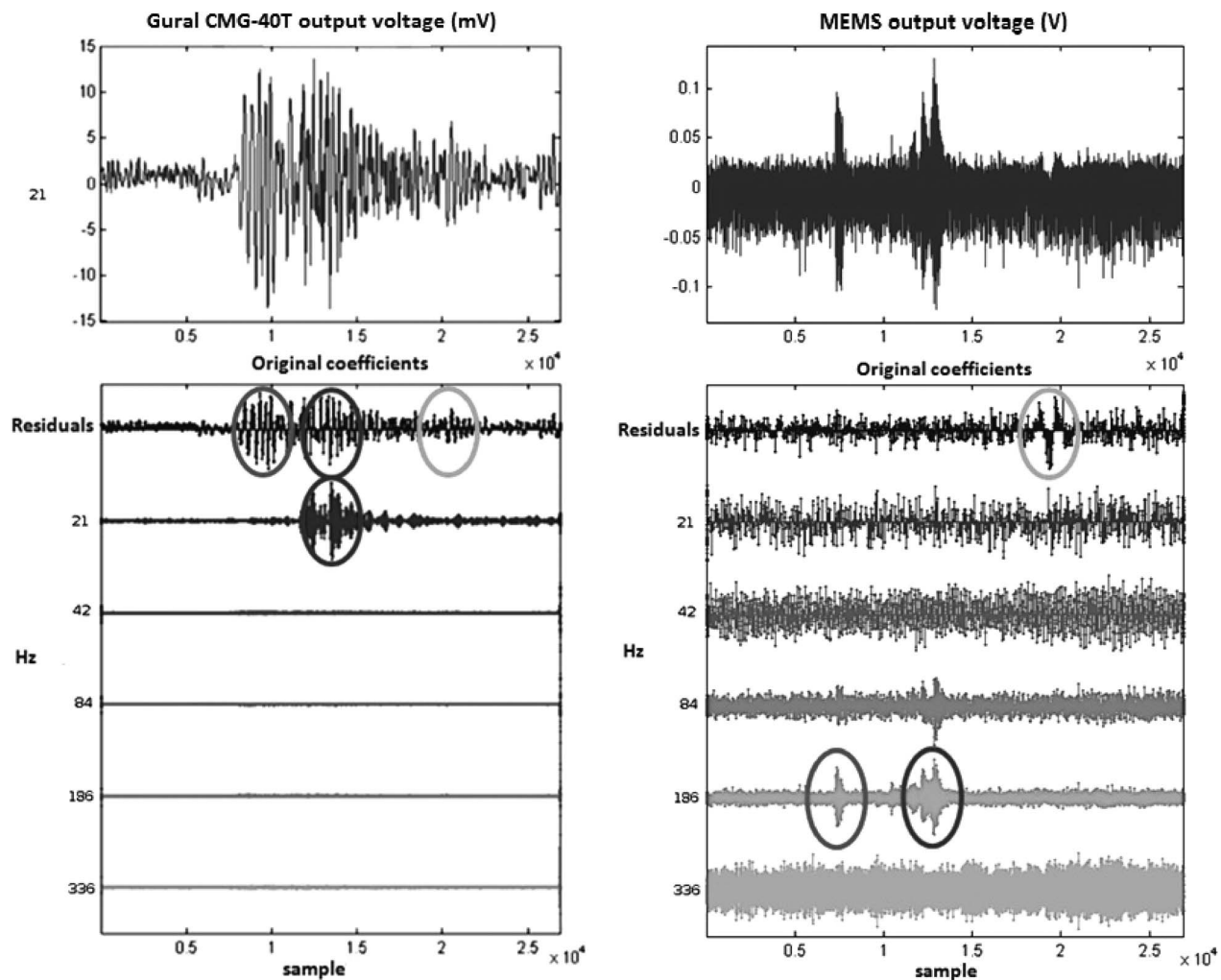


Fig. 10. Results of the wavelet analysis evaluation of the two recorded signals: the Guralp CMG-40T output (in millivolts) and the MEMS output (in volts).

seismic activity. It is interesting to observe that the developed MEMS in terms of sensitivity is comparable with commercial sensors (e.g., the Guralp CMG-40T seismometer). However, it must be stressed that the device is a laboratory prototype, which must be improved to be put into the market and for applications requiring robustness against hostile environments. On-field tests performed on the volcano Stromboli confirmed the expected behavior of the device.

#### ACKNOWLEDGMENT

The authors would like to thank Dr. D. Pecoraro for the precious contribution to this paper and Dr. D. Patanè and his group at the Istituto Nazionale di Geofisica e Vulcanologia, Sezione di Catania, Italy.

#### REFERENCES

- [1] T. Aizawa, S. Ito, T. Kimura, K. Onishi, and T. Matsuoka, "Development of MEMS sensors for seismic survey," in *Proc. SEGJ Expanded Abstract 116th Meet.*, 2007, pp. 79–82.
- [2] T. Aizawa, T. Kimura, T. Matsuoka, T. Taked, and Y. Asano, "Application of MEMS accelerometer to geophysics," *Int. J. JCRM*, vol. 4, no. 2, pp. 1–4, Dec. 2008.
- [3] J. Bernstein, R. Miller, W. Kelley, and P. Ward, "Low-noise MEMS vibration sensor for geophysical applications," *J. Microelectromech. Syst.*, vol. 8, no. 4, pp. 433–438, Dec. 1999.
- [4] R. S. J. Sparks, "Forecasting volcanic eruptions," *Earth Planet. Sci. Lett.*, vol. 210, pp. 1–15, 2003.
- [5] B. A. Chouet, "Long-period volcano seismicity: Its source and use in eruption forecasting," *Nature*, vol. 380, no. 6572, pp. 309–316, Mar. 1996.
- [6] D. Dzurisin, "Volcano geodesy: Challenges and opportunities for the 21st century," *Phil. Trans. R. Soc.*, vol. 358, no. 1770, pp. 1547–1566, May 2000.
- [7] B. Galle, C. Oppenheimer, A. Geyer, A. McGonigle, M. Edmonds, and L. A. Horrocks, "A miniaturised ultraviolet spectrometer for remote sensing of SO<sub>2</sub> fluxes: A new tool for volcano surveillance," *J. Volcanol. Geotherm. Res.*, vol. 119, no. 1–4, pp. 241–254, Jan. 2003.
- [8] D. Carbone, L. Zuccarello, G. Saccorotti, and F. Greco, "Analysis of simultaneous gravity and tremor anomalies observed during the 2002–2003 Etna eruption," *Earth Planet. Sci. Lett.*, vol. 245, no. 3/4, pp. 616–629, May 2006.
- [9] D. Carbone, G. Currenti, and C. Del Negro, "Multiobjective genetic algorithm inversion of ground deformation and gravity changes spanning the 1981 eruption of Etna volcano," *J. Geophys. Res.*, vol. 113, no. B7, pp. B07406-1–B07406-10, Jul. 2008, DOI: 10.1029/2006JB004917.
- [10] D. Carbone, G. Budetta, F. Greco, and H. Rymer, "Combined discrete and continuous gravity observations at Mt. Etna," *J. Volcanol. Geotherm. Res.*, vol. 123, no. 1/2, pp. 123–135, Apr. 2003.
- [11] D. Liu and P. Ning, "Establishing pairwise keys in distributed sensor networks," in *Proc. 10th ACM Conf. Comput. Commun. Security*, 2003, pp. 52–61.
- [12] B. Andò, S. Baglio, N. Savalli, C. Trigona, M. Baù, V. Ferrari, D. Marioli, E. Sardini, and M. Serpelloni, "Development of a contactless resonant

MEMS force sensor in SOI technology,” in *Proc. Eurosensors XXII*, 2008, pp. 421–424.

- [13] B. Andò, S. Baglio, N. Savalli, C. Trigona, D. Marioli, E. Sardini, and M. Serpelloni, “Hybrid telemetric MEMS for high temperature measurements into harsh industrial environments,” in *IEEE I<sup>2</sup>MTC*, 2009, pp. 1423–1428.
- [14] B. Andò, S. Baglio, A. Beninato, and V. Marletta, “An integrated differential inductive sensor implementing bio-immunoassay,” in *Proc. IEEE Biosens.*, 2009.
- [15] B. Andò, S. Baglio, V. Marletta, N. Savalli, C. Trigona, D. Carbone, D. Patanè, S. Rapisarda, and L. Zuccarello, “A BE-SOI MEMS for inertial measurement in geophysical applications,” in *Proc. IEEE I<sup>2</sup>MTC*, pp. 1326–1330.
- [16] G. K. Fedder, “Simulations of Microelectromechanical Systems,” Ph.D. dissertation, Dept. Elect. Eng. Comput. Sci., Univ. California at Berkeley, Berkeley, CA, 1994.
- [17] J. C. Lagarias, J. A. Reeds, M. H. Wright, and P. E. Wright, “Convergence properties of the Nelder–Mead simplex method in low dimensions,” *SIAM J. Optim.*, vol. 9, no. 1, pp. 112–147, 1998.
- [18] [Online]. Available: [www.guralp.com/products/40T](http://www.guralp.com/products/40T)
- [19] S. Calvari, L. Spampinato, L. Lodato, A. J. L. Harris, M. R. Patrick, J. Dehn, M. R. Burton, and D. Andronico, “Chronology and complex volcanic processes during the 2002–2003 flank eruption at Stromboli volcano (Italy) reconstructed from direct observations and surveys with a hand-held thermal camera,” *J. Geophys. Res.*, vol. 110, no. B2, p. B02201-1, Feb. 2005, DOI: 10.1029/2004JB003129.
- [20] B. A. Chouet, P. Dawson, T. Ohminato, M. Martini, G. Saccorotti, F. Giudicepietro, G. De Luca, G. Milana, and R. Scarpa, “Source mechanisms of explosions at Stromboli Volcano, Italy, determined from moment-tensor inversions of very-long-period data,” *J. Geophys. Res.*, vol. 108, no. B1, p. 2019, Jan. 2003, DOI: 10.1029/2002JB001919.
- [21] B. A. Chouet, G. Saccorotti, M. Martini, P. Dawson, G. De Luca, G. Milana, and E. R. Scarpa, “Source and path effects in the wavefields of tremor and explosions at Stromboli volcano, Italy,” *J. Geophys. Res.*, vol. 102, no. B7, pp. 15 129–15 150, 1997.



**Bruno Andò** received the M.S. degree in electronic engineering and the Ph.D. degree in electrical engineering from the Università di Catania, Catania, Italy, in 1994 and 1999, respectively.

From 1999 to 2001, he was a Researcher with the Electrical and Electronic Measurement Group, Dipartimento Elettrico Elettronico e Sistemistico, now the Dipartimento di Ingegneria Elettrica, Elettronica e dei Sistemi, University of Catania, where he has been an Assistant Professor since 2002. He holds several national and international scientific collaborations.

He teaches courses in “measurement theory,” “electronic instrumentations,” and “sensors and transducers.” During his activity, he has coauthored more than 200 scientific papers, presented in international conferences and published in international journals and books. His main research interests are sensor design and optimization, microelectromechanical system and nanosystem, multisensors architecture for Ambient Assisted Living, new materials for sensors, nonlinear techniques for signal processing with particular interest in stochastic resonance and dithering applications, and distributed measurement systems for environmental monitoring.



**Salvatore Baglio** received the “Laurea” and Ph.D. degrees from the University of Catania, Catania, Italy, in 1990 and 1994, respectively.

He was a Lecturer of automatic control theory with the University of Messina, Messina, Italy, and of electronic measurement systems with the University of Catania. Since 1996, he has been with the Dipartimento di Ingegneria Elettrica, Elettronica e dei Sistemi, University of Catania, where he is currently an Associate Professor of electronic instrumentations and measurements. He is a coauthor of several

scientific publications, including papers that were published in international journals or presented at international conferences, and chapters in books. He is also the holder of several U.S. patents. His research interests are mainly focused on measurement methodologies, smart sensors, microsensors, and microsystems.



**Gaetano L'Episcopo** was born in Catania in 1983. He received the B.S. degree in electronics engineering and the M.S. degree in automation and complex system control engineering in 2006 and 2010, respectively, from the University of Catania, Catania, Italy, where he is currently working toward the Ph.D. degree in the Dipartimento di Ingegneria Elettrica, Elettronica e dei Sistemi.

His research interests include microelectromechanical-system devices for sensors and actuators, microgenerators for energy harvesting, and nanotechnology.



**Vincenzo Marletta** received the M.S. degree in 2007 from the University of Catania, Catania, Italy, where he is currently working toward the Ph.D. degree in the Dipartimento di Ingegneria Elettrica, Elettronica e dei Sistemi.

His main research interests include sensor design and characterization, including ferroelectric and multiferroics electric-field sensors, aids for visually impaired people, soft computing methodologies for instrumentation and measuring systems, smart sensors, exploitation of nonlinear dynamics in sensors, microsensors, and microsystems in standard and dedicated technologies.



**Nicolò Savalli** received the M.S. and Ph.D. degrees from the University of Catania, Catania, Italy, in 1999 and in 2003, respectively.

Since 2003, he has been a Lecturer of applied electronic measurements and electrical measurements with the Dipartimento di Ingegneria Elettrica, Elettronica e dei Sistemi, University of Catania, where he is also currently a Research Associate. He has coauthored more than 70 scientific publications, including international journals, international conferences, and national conferences. His main research

interests include soft computing methodologies for instrumentation and measuring systems, smart sensors, material characterization, device applications of nonlinear dynamics, microsensors and microsystems in standard and dedicated technologies, photonic band-gap materials, and optical filters.



**Carlo Trigona** was born in Siracusa, Italy, in December 18, 1981. He received the M.S. degree in automation engineering and control of complex system and the Ph.D. degree in electronic, automation, and control of complex system from the University of Catania, Catania, Italy, in 2006 and 2009, respectively.

He is currently with the Dipartimento di Ingegneria Elettrica, Elettronica e dei Sistemi, University of Catania. He has authored several scientific papers.

His research interests include microsystems and microsensors, fluxgate magnetometers, and analog and digital electronic circuit designs.